

# Confined one-way mode at magnetic domain wall for broadband high-efficiency one-way waveguide, splitter and bender

Xiaogang Zhang,<sup>1,2</sup> Wei Li,<sup>1, a)</sup> and Xunya Jiang<sup>1, b)</sup>

<sup>1)</sup>State Key Laboratory of Functional Materials for Informatics, Shanghai Institute of Microsystem and Information Technology, Chinese Academy of Sciences, Shanghai 200050, China

<sup>2)</sup>Graduate School of Chinese Academy of Sciences, Beijing 100049, People's Republic of China

We find the one-way mode can be well-confined at the magnetic domain wall by the photonic bandgap of gyromagnetic bulk material. Utilizing the well-confined one-way mode at the domain wall, we demonstrate the photonic one-way waveguide, splitter and bender can be realized with simple structures, which are predicted to be high-efficiency, broadband, frequency-independent, reflection-free, crosstalk-proof and robustness against disorder. Additionally, we find that the splitter and bender in our proposal can be transformed into each other with magnetic control, which may have great potential applications in all photonic integrated circuit.

One-way waveguide has been drawn much attention in recent years<sup>1-11</sup>, for their great potential application in all photonic integrated circuit. A popular solution for one-way waveguide is utilizing the gyromagnetic photonic crystal<sup>7,8</sup>, which can support a chiral edge state that exhibits an anomalous unique directionality. Due to the unidirectionality of chiral edge state, the one-way waveguide can be realized via confinement of the surface states<sup>7,8</sup>. Such one-way photonic crystal waveguides with chiral edge state has been proven to exhibit strong robustness against disorder<sup>9,10</sup>. However, the one-way photonic crystal waveguides need complex structures, which may bring more challenges in integrated circuits. In addition, the existing one-way photonic crystal waveguides are all frequency-sensitive. To avoid these difficulties, very recently, another solution for one-way propagation has been proposed<sup>12</sup>, in which a broadband one-way mode (OWM) is predicted to propagate along a magnetic domain wall. However, the cost of the solution is the broadband OWM may be not suitable for one-way waveguide, since the mode extends into the bulk rather than confinement at the domain wall.

In reviewing these existing efforts, we feel desirable to find a design for one-way waveguide that should include at least three characteristics: (I) simple structure; (II) broadband working frequency; and (III) well-confined mode in the waveguide. In this Letter, we will present our design to serve this purpose.

Our design is based on the domain wall. The key of this work is to find a confinement mechanism to localize the broadband OWM at the domain wall. We find the OWM can be confined well at the domain wall via the *photonic bandgap* of bulk material<sup>13,14</sup>, unlike the one-way photonic crystal waveguides<sup>7,8</sup> confining the OWM in waveguide by the photonic bandgap of gyromagnetic photonic crystal.

Utilizing the OWM well-confined at the domain wall, an one-way waveguide with a simple structure and broad-

band working frequency can be realized. Such OWM makes the one-way waveguide high-efficiency and very robust against disorder. Besides one-way waveguide, the OWM localized at domain wall can also be used to design high-efficiency, crosstalk-proof splitters and benders. Additionally, with magnetic controlling, the splitter and bender can be transformed into each other in our proposal, which may have great potential application in all photonic integrated circuit.

Our model for OWM is schematically shown in Fig.1(a), in which a domain wall exists at the interface between two gyromagnetic media such as yttrium-iron-garnet(YIG)<sup>15</sup> at  $x$ - $y$  plane with anti-parallel dc magnetic fields along  $\pm z$ . We use blue area and yellow area to denote  $-z$  and  $+z$  dc magnetic fields respectively in this figure and subsequent figures. According to real YIG material, the relative permittivity  $\epsilon = 15$  and relative permeability would has a gyromagnetic form<sup>15</sup>:

$$\overleftrightarrow{\mu} = \begin{bmatrix} \mu_1 & \pm j\mu_2 & 0 \\ \mp j\mu_2 & \mu_1 & 0 \\ 0 & 0 & 1 \end{bmatrix} \quad (1)$$

where  $\mu_1 = 1 + \frac{\omega_m(\omega_0 - i\alpha\omega)}{(\omega_0 - i\alpha\omega)^2 - \omega^2}$ ,  $\mu_2 = \frac{\omega\omega_m}{[(\omega_0 - i\alpha\omega)^2 - \omega^2]}$ .  $\omega_0 = \gamma H_0$  is the resonance frequency with  $\gamma$  as the gyromagnetic ratio, and  $H_0$  the sum of the external dc magnetic field.  $\alpha$  is the damping coefficient, and  $\omega_m$  is the characteristic circular frequency corresponding to a wavevector  $k_m = \omega_m/c$ .  $\pm$  and  $\mp$  describe the direction of  $H_0$ . In this structure, only TE wave can be formed as an OWM propagating along the domain wall.

In order to illustrate how to confine an OWM at the domain wall via *photonic bandgap*, we study the dispersion relation of bulk modes and OWMs in our structure, by exactly solving the Maxwell equations<sup>13</sup>, and the results are shown in Fig.1(b). In this figure, the solid lines correspond to the OWMs of domain wall. The brown and gray regions correspond to the projected band structure of bulk modes. For the bulk modes, a gap (gray region) exists obviously. Therefore, we can group the OWMs into two types: OWM-I and OWM-II, whose frequency range are respective in the gap and in the band of bulk modes. Comparison OWM-I with OWM-II, their

<sup>a)</sup>Electronic mail: waylee@mail.sim.ac.cn

<sup>b)</sup>Electronic mail: xyjiang@mail.sim.ac.cn

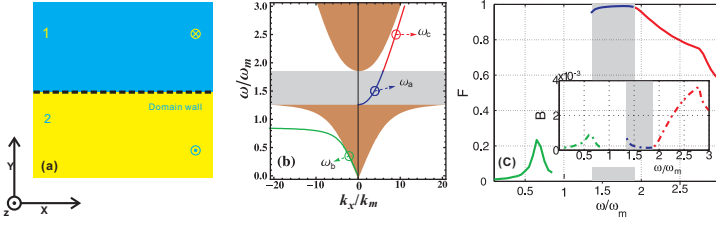


FIG. 1. (a) The model of domain wall. The external dc magnetic field for  $y > 0$  (blue area) and  $y < 0$  (yellow area) are applied along  $-z$  and  $+z$ , respectively. (b) The dispersion relation of TE mode and the projected band structure of bulk modes. The gray and the brown regions represent the photonic bandgap and the extended modes of the bulk respectively. Different OWMs including positive propagation OWM-I, positive propagation OWM-II and negative propagation OWM-II are represented by the blue one, the red one and the green one, respectively. (c) The forward transmission  $F$  (solid lines) and backward transmission  $B$  (dot-dashed lines in the inset box) of OWM-I and OWM-II versus frequency. The distance between the detector and the source is  $100mm$ .

forward transmission<sup>12</sup>  $F$  and backward transmission<sup>12</sup>  $B$  are clearly different, as shown in Fig.1(c). In this figure, we can see the  $F$  and  $B$  of OWM-I (in gray region) are almost unit and zero, respectively, and they are nearly frequency-independent; while for OWM-II, the forward transmission becomes smaller and the backward transmission becomes larger, and both are frequency-dependent. These results indicate that OWM-I is a much higher efficient unidirectional mode. In addition, we can also find that OWM-I is broadband, with working frequency range  $1.28\omega_m$  to  $1.88\omega_m$  ( $\omega_m = 5.26GHz$  in this work).

Physically, the reason that OWM-I exhibits higher efficient unidirectionality than OWM-II can be explained as follows. Only OWM-I can be localized at the domain wall, since it becomes evanescent in the bulk with the intensity decay exponentially away from the domain wall. On the contrary, OWM-II is much easier to extend to the bulk, because their photon energies degenerate with the bulk modes. To show this, three typical OWMs (i.e.,  $OWM_a$ ,  $OWM_b$  and  $OWM_c$  with frequency  $\omega_a=0.3\omega_m$ ,  $\omega_b=1.5\omega_m$  and  $\omega_c=2.5\omega_m$ , respectively) are studied, which are excited by a current source at the domain wall. Obviously,  $OWM_a$  belongs to OWM-I, while  $OWM_b$  and  $OWM_c$  are the type of OWM-II. With a single perfect-electric-conductor (PEC) particle scatter located at the domain wall at a distance  $d = 2mm$  from the source (the scatter is on the right of the source for  $OWM_a$  and  $OWM_c$ , and on the left for  $OWM_b$ ), we calculate the scattered fields of the three OWMs and the radiation patterns of the scatter by Finite-Differential-Time-Domain (FDTD) method<sup>16</sup>, which are shown in Fig.2. From Fig.2(a), we can see the scattered field of  $OWM_a$  is still well-confined at the domain wall, but others extends into bulks as shown in Fig.2(b) and (c). The fact that the confinement quality of OWM-I is much bet-

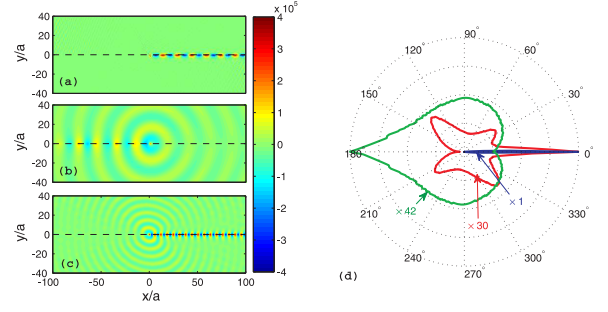


FIG. 2. (a-c) Steady-state scattered fields of  $OWM_a$ ,  $OWM_b$  and  $OWM_c$  scattered by a PEC particle located at the center of domain wall. (d) Radiation pattern. Angular dependence of the energy flux is plotted as a function of polar angle. The  $0^\circ$  and  $180^\circ$  mark  $+x$  and  $-x$  direction, respectively. The blue, green and red lines correspond to the scattered energy flux of  $OWM_a$ ,  $OWM_b$  and  $OWM_c$ , respectively.

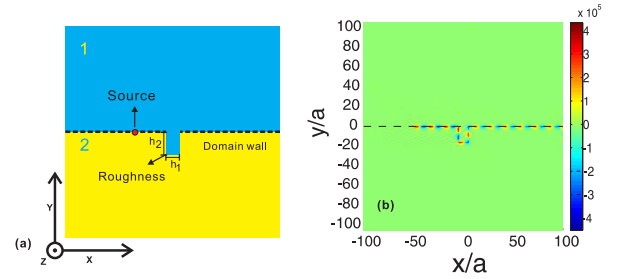


FIG. 3. (a) The structure of the domain wall with roughness. (b) Steady-state  $E_z$  field distribution of  $OWM_a$ .

ter than that of OWM-II can be also illustrated by the radiation pattern of the scatter, as shown in Fig.2(d). In this figure, we can see that only  $OWM_a$  can concentrate almost all energy flux propagating along the domain wall, without reflection and diffraction; while  $OWM_b$  and  $OWM_c$  have quite a bit of energy flux scattered to other directions. With respect to the directional coefficient<sup>17</sup> of the three modes along the domain wall ( $0^\circ$  for  $OWM_a$  and  $OWM_c$ ,  $180^\circ$  for  $OWM_b$ ), we find  $OWM_a$  is about 42 and 30 times larger than that of  $OWM_b$  and  $OWM_c$ , respectively.

Furthermore, such OWM-I is very robust against disorder, since the disorder-induced backscattering is suppressed due to its unidirectionality. This phenomenon is very useful to keep the one-way waveguide high efficiency when the domain wall is rough. To show this in simplicity, as shown in Fig.3(a), a raised portion is chosen to represent the roughness, with  $h_1=10a$  and  $h_2=15a$ , where  $a=1mm$  is the length unit in this work. The OWM of this domain wall with roughness is roused and propagates only along one direction, as shown in Fig.3(b).

As discussed above, OWM-I is very suitable to realize a high-efficiency one-way waveguide. Due to the unidirectionality and well confinement of OWM-I at domain wall, it can also be used to design more devices with simple structures in the realm of all photonic inte-

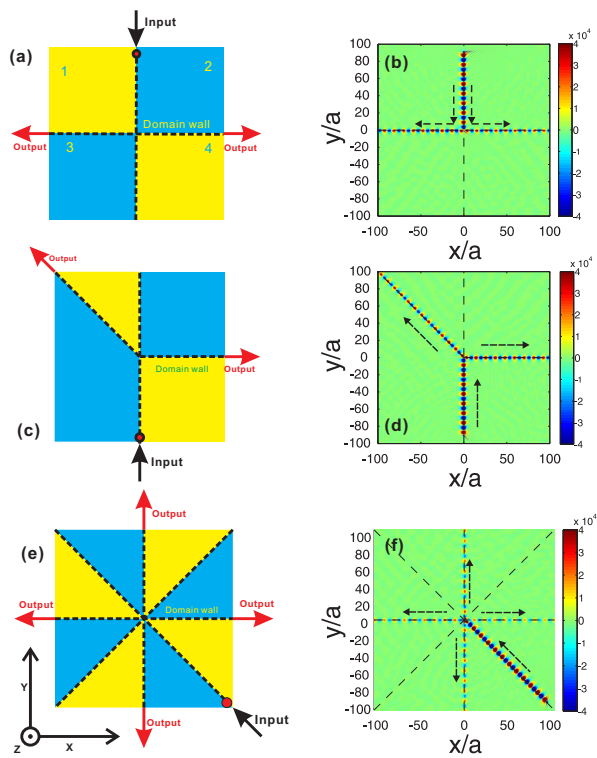


FIG. 4. The structures of splitters and their  $E_z$  field distribution of  $OWM_a$ . (a) 50% beam splitter, and (b) its field distribution. (c) Any-angle beam splitter, and (d) its field distribution. (e) Multiple-beam splitter, and (f) its field distribution. The dashed arrow lines indicate the direction of energy flux.

grated circuit, such as splitter and bender, which are predicted to exhibit high-efficiency, broadband, frequency-independent, reflection-free, crosstalk-proof and robustness against disorder. As typical examples, Fig.4 and Fig.5 show our proposal of splitters and benders, respectively. Our simulation results show that all these devices have the same broadband as the one-way waveguide in Fig.1.

In Fig.4(a), a one-way cross-domain wall splitter based on the domain wall is constituted by four YIG bulks. Utilizing  $OWM-I$ , a beam ( $OWM_a$ ) from the “input” port is split into two equal intensity beams and exit from two “output” ports, as shown in Fig.4(b). It is proved that the splitter is a high-efficiency 50% splitter, since the beams propagating along the domain wall are unidirectional and reflection-free. Furthermore, the beams at different domain walls are immune from crosstalk, because the  $OWM-I$  is well-confined.

Similarly, based on the simple structure of domain wall with  $OWM-I$ , other one-way cross-domain wall splitters can be designed. For instance, an any-angle splitter and a multiple-beam splitter with simple structures, are presented in Fig.4(c) and Fig.4(e), respectively. And their field distributions are shown in Fig.4(d) and Fig.4(f), respectively. From the field distributions, we can find that

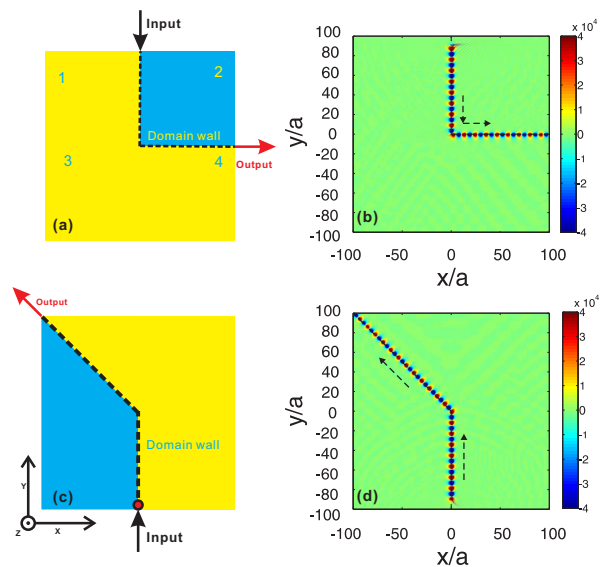


FIG. 5. Benders based on domain wall with  $OWM_a$ . (a)  $90^\circ$  bender, and (b) its  $E_z$  field distribution. (c) Any-angle bender, and (d) its  $E_z$  field distribution of the any-angle bender. The dashed arrow lines indicate the direction of energy flux.

all the splitters exhibit high-efficiency, without reflection, diffraction and crosstalk.

Based upon  $OWM-I$ , we find another important application such as a sharp bender. In Fig.5(a) and Fig.5(c), a  $90^\circ$  bender and an any-angle splitter are illustrated, respectively. Due to  $OWM-I$ , both benders are high-efficiency, which can be seen from the field distributions as shown in Fig.5(b) and (d). Actually, the  $90^\circ$  bender can be transformed from the splitter in Fig.4(a), just by reversing the dc magnetic field direction of area-3 in Fig.4(a), and, the reverse process is also feasible. Following this method, the any-angle bender in Fig.5(c) and the any-angle splitter in Fig.4(c) can also be transformed into each other. The realization of this transformation requires some magnetic control techniques<sup>7,18</sup> such as homogenization and exact location technique. Therefore, with magnetic control, there is a reversible transformation between splitters and benders in our proposal, which may have great potential applications in all photonic integrated circuit.

This work was supported by the NSFC (Grant Nos. 11004212, 11174309, 60877067 and 60938004), and the STCSM (Grant Nos. 11ZR1443800 and 11JC1414500).

- <sup>1</sup>S. Raghu and F. D. M. Haldane, Phys. Rev. A **78**, 033834 (2008).
- <sup>2</sup>H. Takeda and S. John, Phys. Rev. A **78**, 023804 (2008).
- <sup>3</sup>F. Haldane and S. Raghu, Phys. Rev. Lett. **100**, 013904 (2008).
- <sup>4</sup>Z. Yu, Z. Wang, and S. Fan, Appl. Phys. Lett. **90**, 121133 (2007).
- <sup>5</sup>Z. Yu and S. Fan, Appl. Phys. Lett. **94**, 171116 (2009).
- <sup>6</sup>C. He, X. Chen, M. Lu, X. Li, W. Wan, X. Qian, R. Yin, and Y. Chen, Appl. Phys. Lett. **96**, 111111 (2010).
- <sup>7</sup>Z. Wang, Y. Chong, J. Joannopoulos, and M. Soljačić, Nature **461**, 772 (2009).
- <sup>8</sup>Z. Wang, Y. Chong, J. Joannopoulos, and M. Soljačić, Phys. Rev. Lett. **100**, 013905 (2008).

- <sup>9</sup>Z. Yu, G. Veronis, Z. Wang, and S. Fan, Phys. Rev. Lett. **100**, 023902 (2008).
- <sup>10</sup>S. Liu, W. Lu, Z. Lin, and S. Chui, Phys. Rev. B **84**, 045425 (2011).
- <sup>11</sup>X. Xia and J. J. Quinn, Phys. Rev. B **50**, 11187 (1994).
- <sup>12</sup>H. Zhu and C. Jiang, Opt. Express **18**, 6914 (2010).
- <sup>13</sup>See supplementary material.
- <sup>14</sup>A. Hartstein, E. Burstein, A. Maradudin, R. Brewer, and R. Wallis, J. Phys. C: Solid State Phys. **6**, 1266 (1973).
- <sup>15</sup>S. Liu, J. Du, Z. Lin, R. Wu, and S. Chui, Phys. Rev. B **78**, 155101 (2008).
- <sup>16</sup>K. Yee, Antennas and Propagation, IEEE Transactions on **14**, 302 (1966).
- <sup>17</sup>W. L. Stutzman and G. A. Thiele, *Antenna theory and design, 2nd ed.* (John Wiley & Sons, Inc., New York, 1998).
- <sup>18</sup>H. Lee, E. Sun, D. Ham, and R. Weissleder, Nat. Med. **14**, 869 (2008).